Transcriptional Remodeling of the Stromal and Endothelial Microenvironment in MGUS to Multiple Myeloma Progression

Itziar Cenzano[1,2,*], Miguel Cócera[1,3,*], Azari Bantan[2], Marta Larrayoz[1], Amaia Vilas-Zornoza[1,3], Patxi San-Martin[1], Paula Aguirre-Ruiz[1], Diego Alignani[1,3], Aitziber Lopez[1], Marta Miñana Barrios[4], Delia Quilez Agreda[4], Ignacio Sancho González[5], Javier Ruiz[5], Vincenzo Lagani[2,6,7], Jesper Tegner[2,8,9,10], Ignacio Martín-Subero[11,12], Xabier Agirre[1,3], Bruno Paiva[1,3], Paula Rodriguez-Otero[3,13], Luis-Esteban Tamariz-Amador[3,13], Jesús San-Miguel[3,13], Jose A. Martinez-Climent[1,3], Borja Saez[1], Mikel Hernáez[3,14], Isabel A. Calvo[1,3,§], David Gomez-Cabrero[2,15,§], Felipe Prosper[1,3,13,§]

[1]Hematology and Oncology Program, Centre for Applied Medical Research (CIMA), Instituto de Investigaciones Sanitarias de Navarra (IdiSNA), Cancer Center Clinica Universidad de Navarra (CCUN), Pamplona, Spain.
[2]Bioscience Program, Biological and Environmental Sciences and Engineering Division (BESE), King Abdullah University of Science and Technology (KAUST), Thuwal, Saudi Arabia.
[3]Centro de Investigacion Biomedica en Red de Cancer (CIBERONC). Madrid, Spain.
[4]Hospital Reina Sofía de Tudela, Tudela, Spain.
[5]Hospital Universitario de Navarra, Instituto de Investigaciones Sanitarias de Navarra (IdiSNA), Pamplona, Spain.
[6]SDAIA-KAUST Center of Excellence in Data Science and Artificial Intelligence, Thuwal, Saudi Arabia.
[7]Institute of Chemical Biology, Ilia State University, Tbilisi, Georgia.
[8]Computer Science Program, Electrical and Mathematical Sciences and Engineering Division, King Abdullah University of Science and Technology (KAUST), Thuwal, Saudi Arabia.
[9]Unit of Computational Medicine, Department of Medicine, Center for Molecular Medicine, Karolinska Institutet, Karolinska University Hospital, Stockholm, Sweden.
[10]Science for Life Laboratory, Solna, Sweden
[11]Institut d'Investigacions Biomèdiques August Pi i Sunyer (IDIBAPS), Barcelona, Spain.
[12]Institució Catalana de Recerca i Estudis Avançats (ICREA), Barcelona, Spain.
[13]Hematology and Cell Therapy Department. Cancer Center Clinica Universidad de Navarra (CCUN), Instituto de Investigaciones Sanitarias de Navarra (IdiSNA). Pamplona, Spain.
[14]Computational Biology Program. Cima Universidad de Navarra, Data Science and Artificial Intelligence Institute (DATAI) Universidad de Navarra, Instituto de Investigaciones Sanitarias de Navarra (IdiSNA). Pamplona, Spain.
[15]Translational Bioinformatics Unit, Navarrabiomed, Universidad Pública de Navarra (UPNA).

*These authors contributed equally to this work
[§]These authors jointly supervised this work

RUNNING TITLE: scRNA-seq of BM microenvironment in MM progression

KEYWORDS
Multiple myeloma, MGUS, single-cell RNA sequencing, Endothelial cells, Stromal cells, tumor microenvironment.

CORRESPONDING AUTHOR
Felipe Prósper (fprosper@unav.es), David Gomez-Cabrero (david.gomezcabrero@kaust.edu.sa) and Isabel A. Calvo (icalvoa@unav.es).

For original data, please contact (icenzano@unav.es)

ABSTRACT

The role of the bone marrow microenvironment (BME) in the transition from monoclonal gammopathy of undetermined significance (MGUS) into clinically active multiple myeloma (MM) is not completely determined. To address this issue, we performed single-cell RNA sequencing (scRNA-seq) of non-hematopoietic BME cells as well as plasma cells (PC) from two genetically engineered mouse models of MM termed $BI_{c\gamma1}$ and $MI_{c\gamma1}$ that recapitulate the progression of MGUS into MM. Our results identify distinct transcriptional dynamics between endothelial cells (EC) and mesenchymal stem cells (MSC). While EC acquire a stress state during MGUS, a proliferating and angiogenic profile characterizes MM. On the other hand, MSC compromised their differentiation potential, exhibiting a more inflammatory profile that initiates from the MGUS stage. Interestingly, we identified an interferon (IFN)-related myeloma signature in malignant EC of the $BI_{c\gamma1}$ model, which is also expressed in MSC but not observed in the more aggressive $MI_{c\gamma1}$ model and can be identified in MSC from a subgroup of MM patients. The analysis of the EC and MSC interactions with malignant PC revealed stage-specific interactions that contribute to angiogenesis, immunomodulation, and MM extravasation. Finally, the translational relevance of our results in humans was confirmed on MSC from newly diagnosed patients with monoclonal gammopathies at different stages of the disease. In summary, these results show a remodeling of the non-hematopoietic BME in MM progression, providing potential targets at the tumor-niche interface that may hold clinical significance and complement existing immunotherapies.

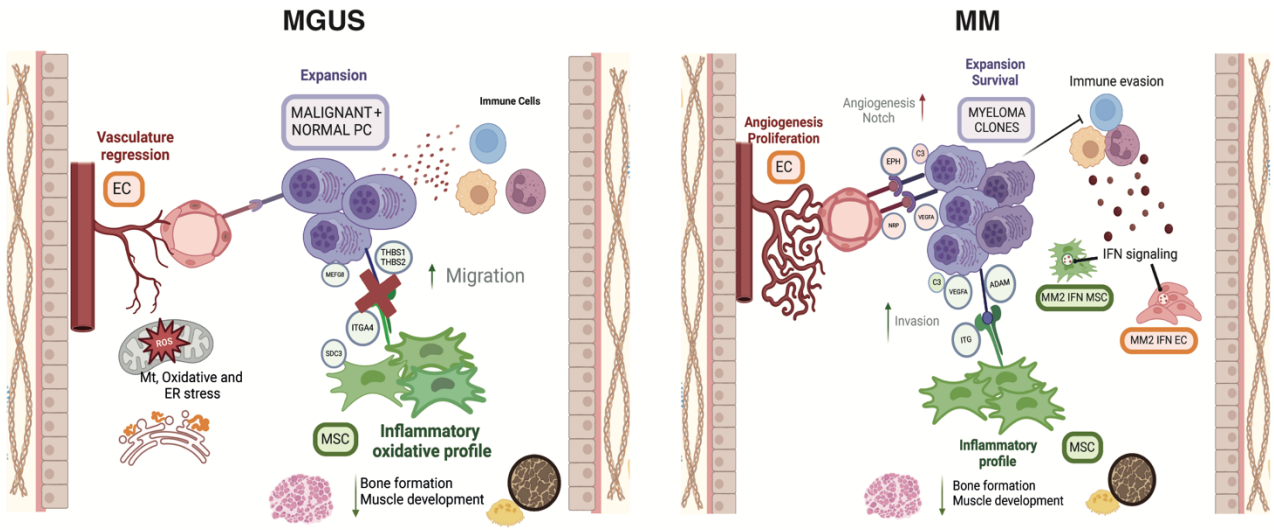

KEY POINTS

- EC stress pre-vascular state in MGUS, shifts to angiogenic in MM, while MSC early transcriptional changes in MGUS persist in overt MM.
- Identification of a myeloma-specific IFN signature in the non-hematopoietic BME that could define a subgroup of MM patients.

INTRODUCTION

Multiple myeloma (MM) is a B-cell malignancy characterized by the clonal expansion and dissemination of plasma cells (PC) in the bone marrow (BM) that is preceded by asymptomatic precursor conditions, namely monoclonal gammopathy of undetermined significance (MGUS) and smoldering multiple myeloma (SMM)[1]. Despite significant improvement in the response and overall survival of MM due to the introduction of novel therapies, patients eventually relapse, and it is still considered an incurable disease[2]. Treatment of the disease at SMM in high-risk patients has been associated with increased progression-free survival and may improve long-term survival. Understanding the molecular mechanism underlying progression from precursor stages to symptomatic MM is thus instrumental in designing therapies directed to prevent development of overt disease.

The BM microenvironment (BME) comprises a complex network of hematopoietic and non-hematopoietic cells, extracellular matrix components, and soluble factors. This microenvironment creates an immunosuppressive and proinflammatory milieu that supports malignant PC growth and survival[3]. Therefore, the intricate interactions between myeloma cells and their surrounding microenvironment are crucial for developing effective therapies that can disrupt supportive signals and overcome drug resistance. While most studies have focused on the immune component[4–7], mounting evidence suggests that endothelial cells (EC) and mesenchymal stem cells (MSC) foster myeloma PC[8,9]. Furthermore, an enhanced inflammatory signature has been identified in MSC of MM patients[10–12]. However, the role of the non-hematopoietic BME in the transition from MGUS to MM remains less understood.

In the current study, we took advantage of our recently described mouse models of MM that recapitulate the clinical, genetic, molecular, and immunological characteristics of MM patients[13]. These models are characterized by the presence of a precursor stage equivalent to MGUS that evolves into asymptomatic MM. We performed single-cell RNA sequencing (scRNA-seq) on Fluorescent-Activated Cell Sorted (FACS) non-hematopoietic BME cells and PC from the same animals.

Our results identified distinct transcriptional changes between EC and MSC during the different stages of the disease. While EC exhibited significant differences between MGUS and MM, changes in MSC are already identified at the MGUS stage, characterized by compromised differentiation and inflammatory profile. Interestingly, we identified an interferon (IFN)-related myeloma signature in both EC and MSC. Our work reveals altered crosstalk between BME cells and malignant PC potentially involved in disease development with a decline in the interactions during the MGUS stage. Finally, we unveil similar transcriptional alterations in MSC from patients with MGUS, SMM, and MM underlying progression into MM.

METHODS

Mice

We used two genetically engineered MM mouse models, $BI_{c\gamma1}$ and $MI_{c1\gamma}$, that recapitulate the most common changes observed in human MM, and $YFPc\gamma_1$ mice were used as controls[13] (see Supplemental Methods). For each scRNA-seq experiment, we used 5-6 mice per control, MGUS, and MM groups. The study included mice of both sexes and was approved by the Ethical Committee of Animal Experimentation of the University of Navarra and the Health Department of the Navarra Government.

Murine BM non-hematopoietic cells were isolated as previously described[14] and sorted with GFP-positive (GFP^+) PC using BD FACSAria II for subsequent scRNA-seq.

Human

BM aspirates from individuals of both sexes with newly diagnosed MGUS (n = 5), SMM (n =2), or MM (n =10), and bone-chip BM samples from healthy donors (HD) (50-80 years of age) undergoing orthopedic surgery were collected. Written informed consent was obtained according to the Declaration of Helsinki and the Institutional Review Board of the University of Navarra. The clinical characteristics of all individuals are described in **supplemental Table 1**.

Samples were processed by lysing red blood cells, and portions of bones were crushed and collagenized. Subsequently, BM cells were cryopreserved with FBS and 10% dimethyl sulfoxide (Sigma) in liquid nitrogen

until use. Frozen samples were thawed, and MSC were prospectively isolated and stored at -80ºC for Bulk RNA sequencing (bulk RNA-seq).

Single-cell RNA and Bulk RNA sequencing

Specifics related to the preparation, sequencing, and analysis of the scRNA-seq and bulk RNA-seq libraries are described in supplemental Methods. scRNA-seq genomic sequence reads were analyzed using the CellRanger suite against the mouse reference genome mm10. Analysis of scRNA-seq was performed using R version (v) 4.1.3 and Seurat v.4.3.0[15]. Additional information, including quality control steps, differential expression, gene set enrichment analysis (GSEA), cell-cell communication, and gene regulatory network (GRN) analysis, are described in supplemental Methods.

RESULTS

Single-cell transcriptomic profiling of BM murine cells in control, MGUS, and MM

The BME is essential for fostering the growth and survival of MM cells. Using the $BI_{c\gamma1}$ myeloma murine model[13], we characterized the influence of the stromal and endothelial BME on disease transformation. This model carrying BCL2 and $IKK2^{NF\text{-}\kappa B}$ genetic lesions develops MGUS starting around 6 months of age and progressing to MM in 4 to 6 months. Considering that $BI_{c\gamma1}$ mice received T-cell-driven immunization, we included similarly immunized $YFP_{c\gamma1}$ mice as controls (**Figure 1A**). Then, we performed scRNA-seq on FACS-sorted non-hematopoietic BME cells (Lin^-, $TER119^-$, $CD45^-$, VDO^+, and $7AAD^-$) and PC (VDO^+, $7AAD^-$ and GFP^+) (**supplemental Figure 1**). After preprocessing, we obtained a total of 17451 cells across all groups (control=2654, MGUS=6122, MM=8675). We identified 19 clusters comprising EC, MSC, PC, and other immune cells from the BME (**Figure 1B**; **supplemental Figure 2A-B**). Based on *Sdc1*, *Xbp1, Tnfrsf17,* and *Slamf7* expression, eight clusters were labeled as PC (clusters 1, 2, 5, 9, 10, 11, 12, 13, n=7924). Clusters 16 and 17 (n=257) expressing *Hba−a1*, *Hba−a2, Hmgb2,* and *Car2* were labeled as erythroblasts. Cluster 18 (n=176), expressing *S100a8*, *S100a9, Fcer1g,* and *Lyz2* was labeled as neutrophils (**Figure 1C; supplemental Figure 2C-D**). EC (clusters 3, 7, 8, n= 3288) were identified by the expression of the canonical markers *Cdh5*, *Cav1*, *Ly6c1*, and *Kdr* (**Figure 1C; supplemental Figure 2C-E**). MSC (clusters 14, 15, n= 592) expressed mesenchymal and osteolineage-primed markers *Cxcl12*, *Pdgfra*, *Lepr*, and *Col1a1* (**Figure 1C; supplemental Figure 2C-F**).

To better understand the roles of MSC and EC in myeloma progression, we conducted a series of confirmatory analyses on both cell populations (**supplemental Figures 2G-J)**. Next, we found an increase in the number of BM EC during MM development, which was verified by flow cytometry (**Figures 1D-E; supplemental Figure 3**). Overall, these results validate our cell enrichment strategy for isolating EC and MSC within the non-hematopoietic BME.

Identification of a myeloma-specific IFN signature in the BME

The observed increase in EC numbers during MM emphasizes a potential connection between EC and MM progression. Delving into the composition of EC, UMAP analysis revealed a cluster of cells shared across all stages alongside a second cluster ("MM2") that was nearly unique to the MM stage, suggesting a central role of the "MM2" cluster in myeloma (**Figure 2A**). The "MM2" cluster was characterized by the expression of IFN-inducible genes such as *Ifit2*, *Rsad2*, *Ifit3*, *Isg15*, *Ifi44, Ifit,* and *Oasl2*, indicating an upregulation of an IFN response (**Figure 2B**), as confirmed by an over-representation analysis (ORA) (**Figure 2C**).

To uncover the mechanisms governing the IFN-like signature, we carried out a GRN analysis using SCENIC[16]. Regulon analysis implicated Irf7, Stat1, and Stat2 as master regulators significantly activated in "MM2" EC (**Figure 2D; supplemental Figure 4A-B**). These transcription factors (TFs) are positive regulators of type 1 IFN, a response linked to T cell immunosuppressive function in myeloma patients[17]. In addition, genes related to T-cell regulation were identified as targets of those regulons (**supplemental Figure 4C**).

To determine whether this IFN-like signature was unique for EC, we evaluated the signature score related to "MM2" EC across other BM populations. This signature was also significantly upregulated in MM in MSC and other BM cells, including PC, neutrophils, and erythroblasts, suggesting a shared immunomodulatory response of the BME to the disease (**Figures 2E-F; supplemental Figure 4D**). As the signature was not

present in control or precursor stages, we termed it MM-IFN signature to emphasize its association with the myeloma phenotype.

Interestingly, when we analyzed the MM-IFN signature in the $MI_{c\gamma1}$ model[13], characterized by rapid MGUS-to-MM transition, we observed no significant enrichment at any stage in either population (**Figure 2G; supplemental Figure 4E**). This finding prompted us to further investigate this MM-IFN signature in humans. The analysis of a publicly available dataset containing MSC from MM patients and HD[11] uncovered an enrichment of the murine MM-IFN signature in a subset of MM patients, independent of genomic alterations (**supplemental Figure 4F-G**). Likewise, previous studies have described a similar IFN signature with highly overlapping genes in PC and immune cells from certain MM patients[4,5]. Collectively, our findings suggest that IFN-signaling is a coordinated response within the BME and could define a subgroup of patients with MM.

EC are characterized by a stress pre-vascular state during MGUS stage

To investigate deeper the molecular mechanisms of myeloma progression, we analyzed the transcriptional changes among the non-IFN EC at the different stages of the disease. An initial analysis uncovered a distinct transcriptome profile of MGUS EC compared to control and MM (**Figure 3A**). Interestingly, MGUS EC overexpressed *Slpi*, *Mt1*, *Mt2*, and *Hspa5*, indicating a stress state at the onset of the disease related to protein folding, reticulum stress, and ion homeostasis (**Figure 3B; supplemental Figure 5A-B; supplemental Table 2**). The upregulation of these genes may be involved in neovessel formation and could represent a "pre-vascular phase" in the progression to MM[18]. Moreover, *Cd74*, *Tmem176a,* and *Nme2*, which are involved in various pathological conditions[19–21], were also overexpressed in MGUS EC (**supplemental Figure 5C**). [19–21]

Then, to comprehend how EC might contribute to disease progression, we performed a differential expression analysis comparing MGUS and MM EC. Overall, we observed 180 differentially expressed genes (DEGs) between both stages (175 upregulated and 5 downregulated) (**Figure 3C; supplemental Table 3**). MM EC revealed angiogenesis, migration, differentiation, and cell proliferation enrichment, reflecting the vascular phenotype (**Figure 3D**). We also found overexpression of lipid metabolism-related genes, reflecting the potential role of lipoproteins in MM[22]. Among the upregulated genes in MM EC, *Sox18* was particularly interesting as it is critical for vascular development in various tumors[23](**supplemental Figure 5D**). *Fabp4* and *Cav1* were also upregulated in MM EC, suggesting their role in malignant transformation.

When expanding our analysis to the $MI_{c\gamma1}$ model, we observed a stress transition state similar to the $BI_{c\gamma1}$ model (**supplemental Figure 6A**). Interestingly, genes upregulated in MGUS-$MI_{c\gamma1}$ EC mirrored those elevated in MM-$BI_{c\gamma1}$ EC, showing an increased vascular phenotype and supporting the rapid disease progression of the $MI_{c\gamma1}$ model (**supplemental Figure 6B**). Likewise, *Anxa2*, *Anxa5*, *S100a6*, and *S100a10* were upregulated in MM-$MI_{c\gamma1}$ EC, which have been associated with a more aggressive disease[24,25](**Figures S6C-F**).

Next, we focused on the GRNs deregulated between MGUS and MM non-IFN EC of the $BI_{c\gamma1}$ model, which better mimics the slower progression observed in humans. The analysis revealed a decline in the activity of certain regulons during disease progression (**Figure 3E; supplemental Figure 7A-B**). Xbp1, shown to promote endothelial proliferation and angiogenesis through VEGF signaling[26], displayed the highest regulon activity in MGUS EC (**Figure 3F; supplemental Figure 7BC**). Furthermore, the overrepresentation of Fos regulon in MGUS and MM EC suggests the importance of this gene in both PC and BM EC[27] (**supplemental Figure 7C**). Interestingly, the ETS family and Sox18 regulons were recovered in MM, suggesting a potential role in disease pathogenesis (**Figure 3F; supplemental Figure 7C**). Globally, our results suggest that MM vascularization is preceded by a stress transition state during MGUS, offering insights into the abnormal regulatory programs driven disease progression in EC.

MSC undergo early transcriptional changes during pre-malignant MGUS that persist in overt MM

Recognizing MSC as crucial contributors to the MM microenvironment, we sought to unravel the transcriptional alterations that arise during myeloma progression in non-IFN MSC. The transcriptional analysis revealed a similar transcriptional profile between MGUS and MM MSC, suggesting that the deregulation associated with the disease begins as early as the premalignant stage in MSC (**Figure 4A**). GSEA revealed impaired osteogenic and adipogenic differentiation capacity in MSC during MM development, in line with previous MM reports[9,10,28] (**Figure 4B; supplemental Table 4**). We also found a downregulation of genes

involved in muscle cell development, including *Pi16*, *Myl6*, *Enpp2, Nupr1*, and *Shox2*, which have not been previously implicated in MM.

As changes were already identified during the MGUS stage, we first compared MSC from MGUS and control (**supplemental Table 5**). MGUS MSC overexpressed oxidative phosphorylation, ATP metabolism, protein folding, and RNA processing-related genes (**Figure 4C-D**). Upregulation of *Cd74* in MGUS MSC and EC suggests its potential role in myeloma progression. Only 35 genes showed differential expression between MM and MGUS MSC (21 upregulated and 14 downregulated) (**Figure 4E; supplemental Table 6**). Functions related to the immune response were the most affected, resembling the inflammatory profile described in MSC from MM patients[11] (**Figure 4F-G**). We analyzed the transcriptional differences in $MI_{c\gamma1}$-MSC and found overlapping DEGs with those seen in the $BI_{c\gamma1}$ model (**supplemental Figure 8**), highlighting the compromised osteogenic, adipogenic, and myogenic differentiation during myeloma development.

Finally, a GRN identified a set of candidate master regulators underlying MSC alteration during disease development (**Figure 4H; supplemental Figure 9A**). Control MSC were enriched in Sp7, Dlx5, Sox8, Sox9, and Cebpa*,* well-known TFs mediating osteochondrogenic and adipogenic differentiation. Moreover, the deregulated activity of Klf4 regulon confirmed the impaired myogenic phenotype of MGUS and MM MSC. TFs from the AP-1 family and Egr1 showed the highest regulon activity in MGUS MSC consistent with their implication in MM development[29,30]. Interestingly, both MGUS and MM MSC showed high levels of Yy1 and Xbp1 regulons, whereas Elk3[31,32] regulon was found to be active only in MM MSC, suggesting a more invasive role (**supplemental Figure 9B-C**). Overall, our results suggest that MSC undergo a transcriptional shift at the MGUS stage that persists along the disease continuum.

Altered crosstalk between EC and MSC with malignant PC is potentially associated to myeloma development
To further understand the mechanism underlying BME-PC communication and how they change upon disease progression, we analyzed cellular communication through LIANA ligand-receptor (L-R) analysis[34] (**Figure 5A**). Focusing our analysis on EC-PC communication, we identified shared interactions in control, MGUS, and MM, as well as disease-stage specific interactions (**supplemental Figure 10A; supplemental Table 7**). The number of interactions decreased during the MGUS stage, followed by an increase in MM (**Figure 5A**). Interactions, through the *Fn1* ligand and *Insr* receptor in EC and the *Cd93* PC receptor, were identified only in controls, while the *Apoe* ligand in EC and the PC *Adam9*, *C3,* and *Vegfa* ligands were only found in MM (**Figure 5B**). Our results support the role of angiogenesis in myeloma progression via *Vegfa* secretion from PC, interacting with *Kdr*, *Nrp1*, and *Nrp2* in EC. Interestingly, high expression of Nrps has been correlated with poor outcomes in multiple cancers[35]. In addition, *Efna1-Epha8* interaction was predicted exclusively in MM, further implicating the ephrin pathway in disease progression (**supplemental Figure 10B**).

We next examined MSC-PC interactions. Interestingly, the L-R analysis between PC and the BME revealed that most interactions are borne from MSC, which declined along disease progression (**Figure 5A; supplemental Figure 10C; supplemental Table 8**). We observed a decrease in *Itga4*-mediated communication, including *Thbs1-Itga4* and *Thbs2-Itga4* interactions that may be related to malignant PC extravasation (**Figure 5C**). MGUS and MM PC participate in different outgoing and incoming interactions not predicted in controls involving *Mfge8* and *Sdc3,* respectively (**Figure 5C; supplemental Figure 10D**). Further analysis of cellular communication revealed interactions related to cell motility and adhesion in MM (**supplemental Figure 10D**). Likewise, *Adam9,* which promotes cancer egress and invasion[37], interacts with MSC through *Itgav* and *Itgb1* in MM (**Figure 5C**).

We uncovered common L-R pairs between EC-PC and MSC-PC along disease progression (**Figure 5D**). Multiple interactions via the *Itgb5* PC receptor were initiated during MGUS. Moreover, malignant PC interacted with both MSC and EC through *Vegfa* secretion, highlighting the role of angiogenesis in MM. Additionally, the interactions of *C3*-mediated responses between PC and the non-hematopoietic BME in MM suggest that *C3* crosstalk may maintain the immunosuppressive environment. Overall, identifying specific BME-PC interactions at different stages of the disease should contribute to improving the understanding of MM development.

Transcriptional dynamics of human MSC during myeloma progression

To validate the results generated with the mouse models, we performed bulk RNA-seq in FACS-isolated MSC obtained from BM samples of aged-matched HD (n = 8), newly diagnosed MGUS (n = 5), SMM (n =2), or MM (n =10) patients (**Figure 6A; supplemental Figure 11**). PCA revealed a distinction between MM-MSC and HD-MSC, with MGUS-MSC and SMM-MSC mapped between them, showing an evolving transcriptional trajectory (**Figure 6B**).

The comparison between MGUS-MSC and HD-MSC revealed 180 DEGs (**supplemental Figure 12A; supplemental Table 9**). Downregulated genes, such as *TNN, SPP1,* and *A2M,* were related to osteoblast differentiation. Besides, MGUS-MSC upregulated genes related to cell cycle, protein folding, ubiquitination, and senescence suppression (**supplemental Figure 12B**). Mitochondrial activity, ATP metabolism, and oxidative stress were also enriched in MGUS-MSC, as previously stated in our mouse data, reinforcing their role in MM pathogenesis.

Consistent with the high transcriptional similarity observed in mice, the fewest DEGs were yielded when comparing MGUS and MM MSC (41 upregulated and 33 downregulated) (**supplemental Figure 12C; supplemental Table 10**). MM-MSC showed enrichment in inflammatory-related processes, suggesting that a pro-inflammatory microenvironment is required to transition from premalignant stages to active myeloma (**supplemental Figure 12D**). In addition, MM-MSC over-expressed *PHLDA1*, *FOXC2*, *PPA1*, and *CTNNB1,* genes associated with Epithelial-Mesenchymal Transition (EMT), which aligns with MSC potential to induce EMT through extracellular vesicles in more aggressive MM[38].

Defective osteogenic differentiation and dysfunctional immunomodulatory ability were confirmed when comparing HD-MSC and MM-MSC (**Figure 6C, supplemental Figure 12E-F; supplemental Table 11**). Furthermore, consistent with the impaired myogenic phenotype observed in mice, human MM-MSC showed downregulation of muscle-related genes (**supplemental Figure 12F**). GSEA revealed enrichment of IFN response and TNF-α signaling via NF-KB in MM-MSC. In addition, the projection of the IFN signature identified previously in the murine MM BME was enriched in a subset of MM patients without any association with genetic alterations (**Figure 6E, supplemental Figure 12G**).

Finally, we determine the changes in TF activity during myeloma progression. Several TFs showed a gradual increase from MGUS to MM-MSC, particularly those related to the NF-KB pathway (**Figure 6F**). Furthermore, MM-MSC exhibited increased activity of *IRF1* and *IRF3*, which again emphasized the importance of IFN signaling for the disease. In conclusion, the transcriptional reprogramming of MSC along the disease continuum supports a consistent pattern shared by both human patients and mouse models.

DISCUSSION

Over the last decades, our understanding of MM biology has advanced significantly, with scRNA-seq analysis driving profound insights into MM heterogeneity, tumorigenesis, and extramedullary metastasis[39–43]. An important part of this novel understanding is the evidence that the BME contributes to the outgrowth and relapse of this neoplasia and exerts a supportive function for the expansion of malignant PC[4,11,44,45]. However, research has mainly concentrated on PC and their immune microenvironment, highlighting the need for additional exploration of the non-hematopoietic BME. Here, using our $BI_{c\gamma1}$ and $MI_{c\gamma1}$ murine models[13], which mirror MM pathogenesis, we provide a comprehensive overview of the transcriptional deregulation within EC and MSC during the transition from healthy to MGUS and MM. Our single-cell analysis has revealed the longitudinal transcriptional alterations of the BME during MM development and the dynamic interplay between PC, EC, and MSC. Moreover, using bulk RNA-seq of MSC from MGUS, SMM, and MM patients, we observe consistent transcriptional reprogramming of MSC across human patients and mouse models.

A fundamental finding of our study is the identification of a myeloma-specific IFN signature in EC that extends to MSC and other BM populations, suggesting a shared response of the BME during myeloma progression. While IFN-related signature has been reported in PC and the immune environment[4,5,46], our data reveal that, in fact, non-hematopoietic cells exhibit this IFN fingerprint marked by the upregulation of IFN-inducible genes and the master regulators *Irf7*, *Stat1*, and *Stat2*. Previous studies highlighted *STAT3* as an oncogenic driver in MM and reported the role of *STAT1* in promoting MM migration and BM homing[47]. The heightened correlation

between Stat signaling and IFN in MM EC and MSC expands the emerging tumor-promoting roles described for Stat1 and Stat2 pathways.

This IFN-inducible signature suggests an active response pathway and unveils a new immunomodulatory potential within the non-hematopoietic BME. We speculate that EC and MSC reprogramming into IFN-inducible signaling may contribute to the remodeling of immune functions, promoting T-cell exhaustion under inflammatory conditions[17]. Extending our observations to humans, we reinforce the relevance and applicability of the identified MM-IFN signature to the clinical setting. The enrichment of the murine IFN fingerprint in MSC from a subset of MM patients may help to define a narrower patient group within the MM heterogeneity, particularly relevant in patients with a more inflammatory component.

Examining the molecular mechanisms governing myeloma progression within non-IFN EC identified transcriptional and regulatory changes during MGUS related to protein folding and ion homeostasis. The upregulation of *Slpi*, *Mt1*, *Mt2*, and *Hspa5*, known for their roles in tumor angiogenesis and pro-survival signaling[49,50] may serve as promising early indicators of myeloma development in EC. Comparison of MGUS and MM EC reveals dynamic changes associated with disease progression, including angiogenesis, migration, and lipid metabolism, reflecting the vascular phenotype and metabolic alterations characteristic of MM EC. The upregulation of *Sox18*, a key regulator of vasculature development and cancer progression[23], in MM EC highlights its targeting potential.

Unlike EC, transcriptional changes in MSC were already present during the MGUS stage, mirroring those seen in advanced MM, including impairment in osteogenic and adipogenic differentiation, as previously reported[9,10]. Thereby, MGUS MSC may exhibit a reshaping of their differentiation capacity and metabolism to support MM cell growth early in the disease[51]. In a recent study, De Jong et al. identified a sub-population of MSC exhibiting an inflammatory signature in MM patients [11]. Building upon these findings, we observed the enrichment of cytokines, TNFα, and NF-κB pathways, supporting the contribution of MM MSC to the pro-inflammatory tumor microenvironment. Additionally, the upregulation of type 1 IFN in MM MSC reinforces the role of IFN signaling in disease progression. The regulation of MGUS MSC by Egr1 and AP-1 TFs[29,30] and the involvement of Elk3 regulon in maintaining an invasive phenotype in MM highlight the complex networks underlying disease pathogenesis, making them potential biomarkers and therapeutic targets for MM.

Understanding the intricate crosstalk between the BME and PC is crucial for unraveling the mechanisms underlying tumor progression. Our analysis identified a tapestry of interactions targeting myeloma cells and their surrounding microenvironment, shaping the landscape from MGUS to MM. To our knowledge, this study represents the first investigation into the interactions between EC, MSC, and malignant PC along the disease continuum. As the disease progresses, EC-PC communication declines in MGUS and restores in MM, highlighting their evolving relationship. Interactions involving *Vegfa* secretion from PC with *Kdr*, *Nrp1*, and *Nrp2* endothelial receptors emphasize the importance of angiogenesis as an MM hallmark. Additionally, identifying *Efna1-Epha8* interaction exclusively in MM implicates the ephrin pathway in disease development, as previously described in other cancers[52]. Remarkably, MSC-PC interactions were associated with adhesion, matrix organization, and migration, suggesting their crucial role in promoting MM extravasation, emphasizing the role of MSC-PC crosstalk as a potential contributor to the dissemination of the disease.

Challenges associated with the BM EC and stromal scarcity hinder human scRNA-seq studies. Our bulk RNA-seq showed compromised differentiation capacities in MSC from human patients, which, in line with our findings in mice, is also apparent in the premalignant stages. Similarly, MGUS prompts a metabolic swift in human MSC with increased protein folding. Human MM-MSC exhibit higher expression of inflammation-related genes, potentially aiding in immune evasion of MM by suppressing T cells, which could be enhanced by overexpressing *LGALS9* or *FADD*[53,54]. On the contrary, some matrix-related genes, including *SDC2*, *SDC4*, *MMP14,* and *LAMC1,* showed discrepancies between both species that could be attributed to the heterogeneity of MM patients and their different clinical characteristics. Notably, the mentioned genes are linked to patients with poor outcomes, which might not align with the characteristics of our mouse $BI_{c\gamma1}$ model.

In summary, the utilization of the $BI_{c\gamma1}$ myeloma murine model, which recapitulates the progression from MGUS to full-blown MM, coupled with the utilization of scRNA-seq, enables a comprehensive dissection of

the non-hematopoietic BME. The myeloma-specific IFN signature, the transition stress state in MGUS EC, the early transcriptional shifts in MSC, and the evolving cellular communication networks collectively reinforce the role of EC and MSC in MM development. Additionally, validating our murine model findings in human patients strengthens the translational relevance of our study and emphasizes the importance of investigating the mechanisms underlying disease progression. Overall, these results suggest that changes in the non-hematopoietic BME could create a more permissive microenvironment that favors the development of MM from premalignant stages.

ACKNOWLEDGEMENTS
This work was supported by the Instituto de Salud Carlos III and co-financed by ERDF A way of making Europe (PI20/01308, PI23/00516); CIBERONC (CB16/12/00489), RICORS TERAV (RD21/0017/0009); Departamento de Industria Gobierno de Navarra (AGATA 0011-1411-2020-000010/0011-1411-2020-000011) and Departamento de Salud Gobierno de Navarra; the Cancer Research UK [C355/A26819]; FC AECC and AIRC under the Accelerator Award Program; The International Myeloma Foundation (Brian van Novis) and The Paula and Rodger Riney Foundation to FP. The study was also supported by The Spanish Government, through project PID2019-111192GA-I00 (MICINN) to DGC. IAC was supported by Marie Curie grant (H2020- MSCA-IF-837491) from European Commission. IC was supported by AECC predoctoral fellowship (PRDNA19006CENZ). MC was supported by FPU fellowship (FPU22/03283) from Ministerio de Ciencia, Innovación y Universidades.

We would like to thank the staff of the flow cytometry core, the advanced genomic lab, and the animal facility at CIMA Universidad de Navarra for their invaluable technical and intellectual assistance. We also acknowledge Hospital Reina Sofía de Tudela, Hospital Universitario de Navarra, the Biobank of the University of Navarra, and Goretti Ariz for the provision of BM samples and their collaboration. We are particularly grateful to the patients and healthy donors for their participation in this study.

AUTHORSHIP CONTRIBUTIONS
I.C. and M.C. processed murine and human BM samples. I.C. conceptualized the study, analyzed and interpreted the scRNA-seq experiments data, and wrote the paper; M.C. analyzed and interpreted the bulk RNA-seq experiments data; A.B. performed the cell-cell computational analysis; M.L. and J.A.M.C. designed and provided the mice models; A.V., P.S.M., and P.A.R. performed the scRNA-seq and bulk RNA-seq experiments. D.A. and A.L. performed the FACS sorting. M.M.B., D.Q.A., I.S.G., and J.R. provided the BM samples from HD; P.R.O. and L.E.T.A provided the BM samples from MGUS, SMM, and MM patients; D.G.C., with help from M.H., I.M.S, supervised the computational work; I.A.C. and B.S. designed the research experiments; F.P., D.G.C. and I.A.C conceived and directed the research project.
All authors actively participated in the discussions underlying this manuscript. I.C., M.C., I.A.C., D.G.C., and F.P. discussed the results and wrote the final manuscript. All authors contributed to, read, and approved the final manuscript.

DISCLOSURE OF CONFLICTS OF INTEREST
A patent on the knowhow and experimental use of the $BI_{c\gamma1}$ and $MI_{c\gamma1}$ mouse models of MM has been licensed to MIMO Biosciences. The authors declare no competing interests.

REFERENCES

1. Kumar SK, Rajkumar V, Kyle RA, et al. Multiple myeloma. *Nat Rev Dis Primers*. 2017;3(1):17046.
2. Mateos M-V, Nooka AK, Larson SM. Moving Toward a Cure for Myeloma. *American Society of Clinical Oncology Educational Book*. 2022;(42):643–654.
3. Lomas OC, Tahri S, Ghobrial IM. The microenvironment in myeloma. *Curr Opin Oncol*. 2020;32(2):170–175.
4. Zavidij O, Haradhvala NJ, Mouhieddine TH, et al. Single-cell RNA sequencing reveals compromised immune microenvironment in precursor stages of multiple myeloma. *Nature Cancer 2020 1:5*. 2020;1(5):493–506.
5. Boiarsky R, Haradhvala NJ, Alberge JB, et al. Single cell characterization of myeloma and its precursor conditions reveals transcriptional signatures of early tumorigenesis. *Nature Communications 2022 13:1*. 2022;13(1):1–15.
6. Pilcher W, Thomas BE, Bhasin SS, et al. Cross center single-cell RNA sequencing study of the immune microenvironment in rapid progressing multiple myeloma. *npj Genomic Medicine 2023 8:1*. 2023;8(1):1–18.
7. Chen M, Wan Y, Li X, et al. Dynamic single-cell RNA-seq analysis reveals distinct tumor program associated with microenvironmental remodeling and drug sensitivity in multiple myeloma. *Cell Biosci*. 2023;13(1):1–18.
8. García-Ortiz A, Rodríguez-García Y, Encinas J, et al. The Role of Tumor Microenvironment in Multiple Myeloma Development and Progression. *Cancers (Basel)*. 2021;13(2):217.
9. Maiso P, Mogollón P, Ocio EM, Garayoa M. Bone Marrow Mesenchymal Stromal Cells in Multiple Myeloma: Their Role as Active Contributors to Myeloma Progression. *Cancers 2021, Vol. 13, Page 2542*. 2021;13(11):2542.
10. Alameda D, Saez B, Lara-Astiaso D, et al. Characterization of freshly isolated bone marrow mesenchymal stromal cells from healthy donors and patients with multiple myeloma: transcriptional modulation of the microenvironment. *Haematologica*. 2020;105(9):e470.
11. de Jong MME, Kellermayer Z, Papazian N, et al. The multiple myeloma microenvironment is defined by an inflammatory stromal cell landscape. *Nature Immunology 2021 22:6*. 2021;22(6):769–780.
12. de Jong MME, Fokkema C, Papazian N, et al. An IL-1β-driven neutrophil–stromal cell axis fosters a BAFF-rich protumor microenvironment in individuals with multiple myeloma. *Nature Immunology 2024*. 2024;1–14.
13. Larrayoz M, Garcia-Barchino MJ, Celay J, et al. Preclinical models for prediction of immunotherapy outcomes and immune evasion mechanisms in genetically heterogeneous multiple myeloma. *Nat Med*. 2023;29(3):632–645.
14. Ye J, Calvo IA, Cenzano I, et al. Deconvolution of the hematopoietic stem cell microenvironment reveals a high degree of specialization and conservation. *iScience*. 2022;25(5):104225.
15. Stuart T, Butler A, Hoffman P, et al. Comprehensive Integration of Single-Cell Data. *Cell*. 2019;177(7):1888-1902.e21.
16. Aibar S, González-Blas CB, Moerman T, et al. SCENIC: Single-cell regulatory network inference and clustering. *Nat Methods*. 2017;14(11):1083.
17. Sumida TS, Dulberg S, Schupp JC, et al. Type I interferon transcriptional network regulates expression of coinhibitory receptors in human T cells. *Nature Immunology 2022 23:4*. 2022;23(4):632–642.
18. Binet F, Sapieha P. ER Stress and Angiogenesis. *Cell Metab*. 2015;22(4):560–575.

19. Le Hiress M, Tu L, Ricard N, et al. Proinflammatory signature of the dysfunctional endothelium in pulmonary hypertension role of the macrophage migration inhibitory factor/CD74 complex. *Am J Respir Crit Care Med*. 2015;192(8):983–997.
20. Ye C, Ren S, Sadula A, et al. The expression characteristics of transmembrane protein genes in pancreatic ductal adenocarcinoma through comprehensive analysis of bulk and single-cell RNA sequence. *Front Oncol*. 2023;13:1047377.
21. Bai W, Wang H, Bai H. Identification of Candidate Genes and Therapeutic Agents for Light Chain Amyloidosis Based on Bioinformatics Approach. *Pharmgenomics Pers Med*. 2019;12:387.
22. Lazaris V, Hatziri A, Symeonidis A, Kypreos KE. The Lipoprotein Transport System in the Pathogenesis of Multiple Myeloma: Advances and Challenges. *Front Oncol*. 2021;11:638288.
23. Olbromski M, Podhorska-Okołów M, Dzięgiel P. Role of the SOX18 protein in neoplastic processes. *Oncol Lett*. 2018;16(2):1383.
24. Ismail NH, Mussa A, Al-Khreisat MJ, et al. Proteomic Alteration in the Progression of Multiple Myeloma: A Comprehensive Review. *Diagnostics 2023, Vol. 13, Page 2328*. 2023;13(14):2328.
25. Liu M, Wang Y, Miettinen JJ, et al. S100 Calcium Binding Protein Family Members Associate With Poor Patient Outcome and Response to Proteasome Inhibition in Multiple Myeloma. *Front Cell Dev Biol*. 2021;9:.
26. Yang J, Xu J, Danniel M, et al. The interaction between XBP1 and eNOS contributes to endothelial cell migration. *Exp Cell Res*. 2018;363(2):262–270.
27. Jin Y, Chen K, De Paepe A, et al. Active enhancer and chromatin accessibility landscapes chart the regulatory network of primary multiple myeloma. *Blood*. 2018;131(19):2138–2150.
28. Fairfield H, Costa S, Falank C, et al. Multiple Myeloma Cells Alter Adipogenesis, Increase Senescence-Related and Inflammatory Gene Transcript Expression, and Alter Metabolism in Preadipocytes. *Front Oncol*. 2021;10:1.
29. Fan F, Podar K. The Role of AP-1 Transcription Factors in Plasma Cell Biology and Multiple Myeloma Pathophysiology. *Cancers (Basel)*. 2021;13(10):.
30. Chen L, Wang S, Zhou Y, et al. Identification of early growth response protein 1 (EGR-1) as a novel target for JUN-induced apoptosis in multiple myeloma. *Blood*. 2010;115(1):61–70.
31. Huerta-Yepez S, Liu H, Baritaki S, et al. Overexpression of Yin Yang 1 in bone marrow-derived human multiple myeloma and its clinical significance. *Int J Oncol*. 2014;45(3):1184–1192.
32. Xu G, Liu K, Anderson J, et al. Expression of XBP1s in bone marrow stromal cells is critical for myeloma cell growth and osteoclast formation. *Blood*. 2012;119(18):4205.
33. Lee M, Cho HJ, Park KS, Jung HY. ELK3 Controls Gastric Cancer Cell Migration and Invasion by Regulating ECM Remodeling-Related Genes. *Int J Mol Sci*. 2022;23(7):.
34. Dimitrov D, Türei D, Garrido-Rodriguez M, et al. Comparison of methods and resources for cell-cell communication inference from single-cell RNA-Seq data. *Nature Communications 2022 13:1*. 2022;13(1):1–13.
35. Benwell CJ, Johnson RT, Taylor JAGE, Price CA, Robinson SD. Endothelial VEGFR Coreceptors Neuropilin-1 and Neuropilin-2 Are Essential for Tumor Angiogenesis. *Cancer Research Communications*. 2022;2(12):1626–1640.
36. Jinushi M, Nakazaki Y, Carrasco DR, et al. Milk fat globule EGF-8 promotes melanoma progression through coordinated Akt and twist signaling in the tumor microenvironment. *Cancer Res*. 2008;68(21):8889–8898.

37. Fan X, Wang Y, Zhang C, et al. ADAM9 Expression Is Associate with Glioma Tumor Grade and Histological Type, and Acts as a Prognostic Factor in Lower-Grade Gliomas. *Int J Mol Sci*. 2016;17(9):.
38. Kletukhina S, Neustroeva O, James V, Rizvanov A, Gomzikova M. Role of Mesenchymal Stem Cell-Derived Extracellular Vesicles in Epithelial–Mesenchymal Transition. *Int J Mol Sci*. 2019;20(19):4813.
39. Cohen YC, Zada M, Wang SY, et al. Identification of resistance pathways and therapeutic targets in relapsed multiple myeloma patients through single-cell sequencing. *Nature Medicine 2021 27:3*. 2021;27(3):491–503.
40. Ledergor G, Weiner A, Zada M, et al. Single cell dissection of plasma cell heterogeneity in symptomatic and asymptomatic myeloma. *Nature Medicine 2018 24:12*. 2018;24(12):1867–1876.
41. Dutta AK, Alberge JB, Sklavenitis-Pistofidis R, et al. Single-cell profiling of tumour evolution in multiple myeloma — opportunities for precision medicine. *Nature Reviews Clinical Oncology 2022 19:4*. 2022;19(4):223–236.
42. Samur MK, Szalat R, Munshi NC. Single-cell profiling in multiple myeloma: insights, problems, and promises. *Blood*. 2023;142(4):313–324.
43. Tirier SM, Mallm JP, Steiger S, et al. Subclone-specific microenvironmental impact and drug response in refractory multiple myeloma revealed by single-cell transcriptomics. *Nature Communications 2021 12:1*. 2021;12(1):1–16.
44. John L, Poos AM, Brobeil A, et al. Resolving the spatial architecture of myeloma and its microenvironment at the single-cell level. *Nature Communications 2023 14:1*. 2023;14(1):1–17.
45. Sharma NS, Choudhary B. Good Cop, Bad Cop: Profiling the Immune Landscape in Multiple Myeloma. *Biomolecules*. 2023;13(11):.
46. Kellermayer Z, Tahri S, Jong MME de, et al. Immune-mediated tumor control in the 5TGM1 transfer model of multiple myeloma. *bioRxiv*. 2023;2023.01.18.524505.
47. Chong PSY, Chng WJ, de Mel S. STAT3: A Promising Therapeutic Target in Multiple Myeloma. *Cancers (Basel)*. 2019;11(5):.
48. Hazrati A, Malekpour K, Khorramdelazad H, Rajaei S, Hashemi SM. Therapeutic and immunomodulatory potentials of mesenchymal stromal/stem cells and immune checkpoints related molecules. *Biomarker Research 2024 12:1*. 2024;12(1):1–26.
49. Zhu Y, Chang S, Liu J, Wang B. Identification of a novel cuproptosis-related gene signature for multiple myeloma diagnosis. *Immun Inflamm Dis*. 2023;11(11):e1058.
50. Si M, Lang J. The roles of metallothioneins in carcinogenesis. *J Hematol Oncol*. 2018;11(1):.
51. Zhan X, Yu W, Franqui-Machin R, et al. Alteration of mitochondrial biogenesis promotes disease progression in multiple myeloma. *Oncotarget*. 2017;8(67):111213–111224.
52. Pergaris A, Danas E, Goutas D, et al. The Clinical Impact of the EPH/Ephrin System in Cancer: Unwinding the Thread. *Int J Mol Sci*. 2021;22(16):.
53. Akiyama K, Chen C, Wang D, et al. Mesenchymal-Stem-Cell-Induced Immunoregulation Involves FAS-Ligand-/FAS-Mediated T Cell Apoptosis. *Cell Stem Cell*. 2012;10(5):544–555.
54. Kim S, Lee H-J, Jeon M-S, Yi T, Song SU. Galectin-9 is Involved in Immunosuppression Mediated by Human Bone Marrow-derived Clonal Mesenchymal Stem Cells. *Immune Netw*. 2015;15(5):241.

FIGURE LEGENDS

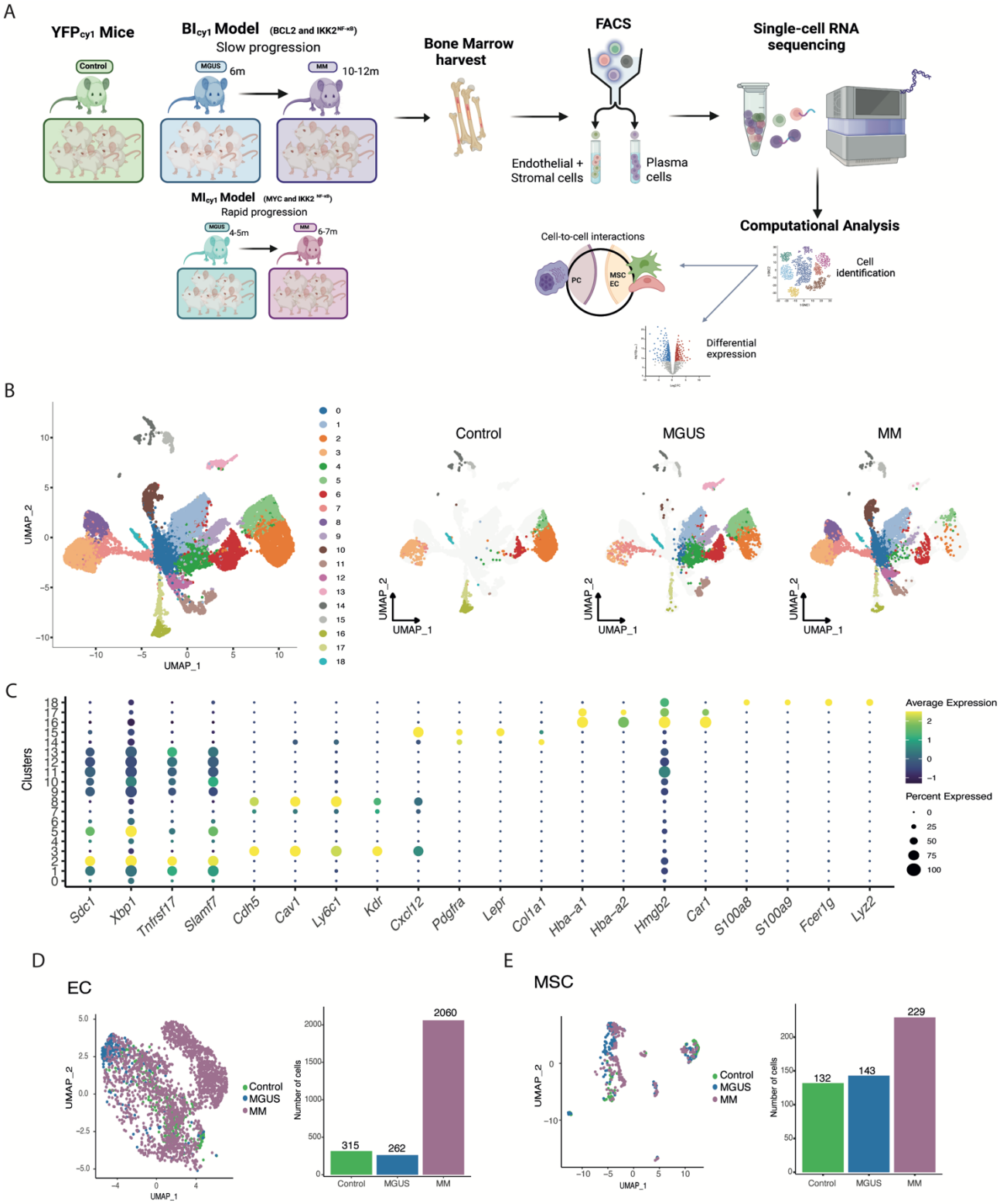

Figure 1. Single-cell transcriptomic profiling of BM murine cells in control, MGUS, and MM. (A) Experiment overview. Schematic view of control, BIcγ1, and MIcγ1 mice and experimental workflow for the isolation and scRNA-seq analysis of PC and BM MSC and EC cells. (B) UMAP representation of murine BME control, MGUS, and MM cells colored by cell clustering after merging samples. Right panels: Original UMAP split into control, MGUS, and MM datasets. (C) Dot plot of canonical markers used to define PC, EC, MSC, erythroblasts, and neutrophils. The dot size reflects the percentage of cells within the cluster expressing each gene, and the color represents the average expression level. (D-E) Left panel: UMAP projection showing

the distribution of control, MGUS, and MM cells for EC (D) and MSC (E). Right panel: Bar plot depicting the total number of cells per stage for EC (D) and MSC (E).

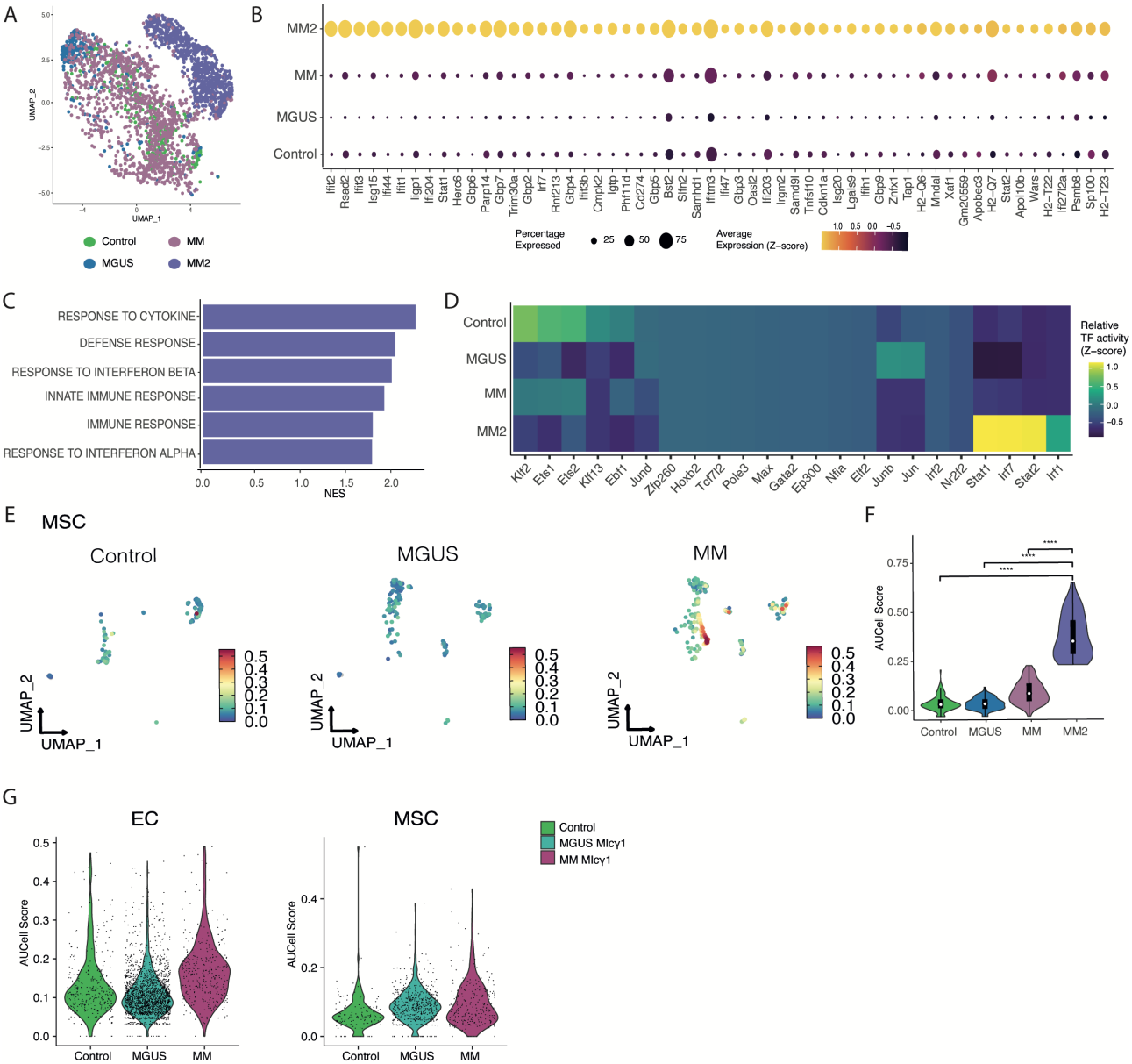

Figure 2. Identification of a myeloma-specific IFN signature in the BME. (A) UMAP dimension reduction of EC revealing a transcriptionally distinct population in MM. (B) Dot plot visualization of the markers defining EC MM2 cluster. Average gene expression is shown by color intensity, and the percentage of cells expressing each gene is shown by size. (C) Bar charts of enriched Gene Ontology (GO) terms from GSEA (FDR < 0.05) computed using MM2 cluster markers. The horizontal axis represents the normalized enrichment score (NES). (D) Heatmap representing z-scaled mean regulon activity score of inferred top specific regulons for each stage. (E) UMAP plot illustrating the distribution of the IFN-related signature in MSC across control, MGUS, and MM. (F) Violin plots showing AUC-score for IFN-related signature within MSC in control, MGUS, MM, and MM2 cells. (G) Violin plots of the AUC-score for IFN-related signature within EC (left panel) and MSC (right panel) in control, MGUS, and MM cells from the MIcγ$_1$ model.

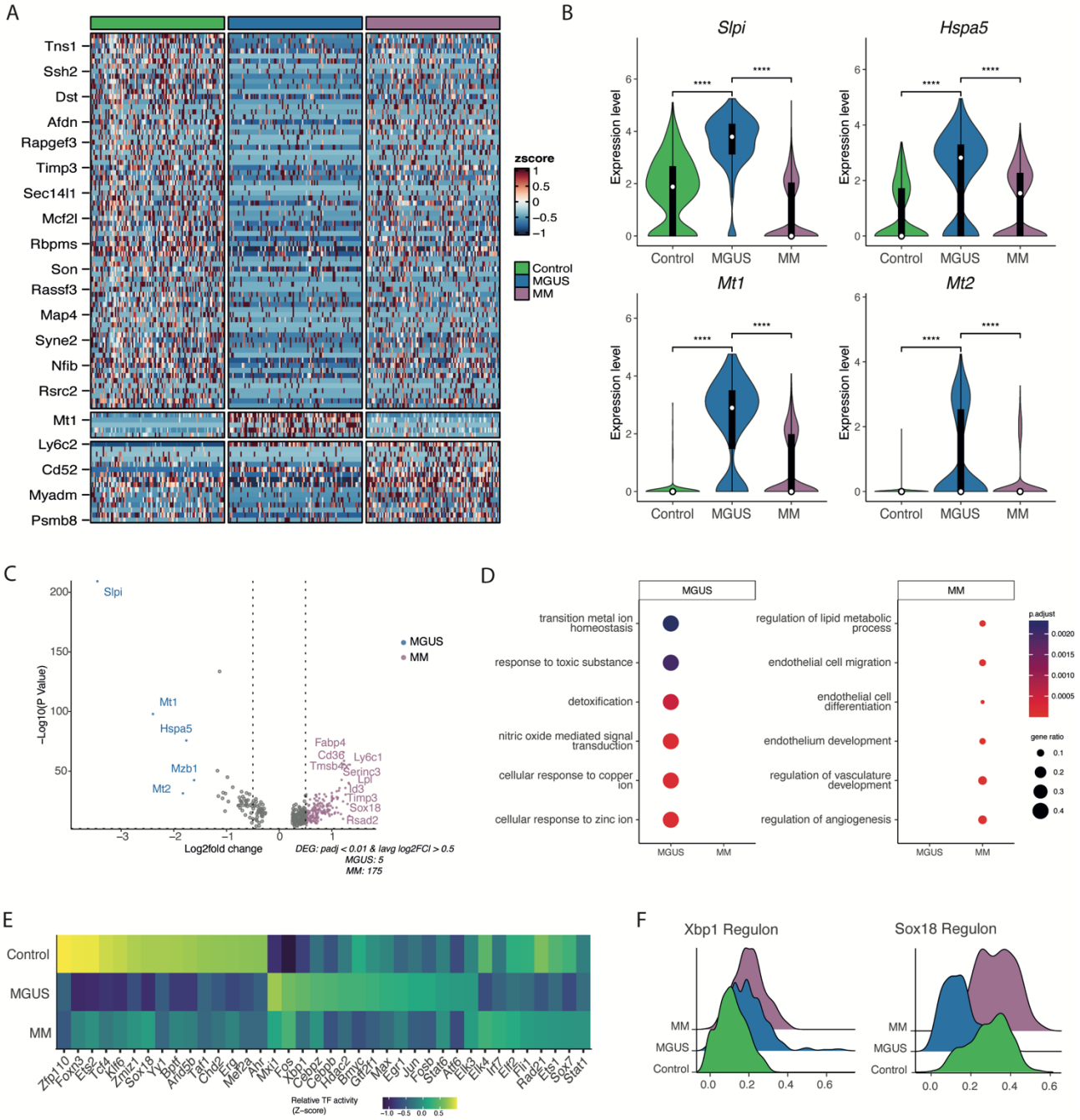

Figure 3. EC are characterized by a stress pre-vascular state during MGUS stage. (A) Heatmap of the DEG between control, MGUS, and MM cells. Color represents the z-score scaled expression values. (B) Violin plots showing the distribution of expression of genes upregulated in MGUS EC. (C) Volcano plot of the DEGs in MGUS vs. MM EC. The y-axis represents the -log10(p-value) and the x-axis represents the log2(fold change). The dot's color denotes the disease stage for which DEG was detected, with grey dots representing non-significant genes. (D) Significant terms derived from ORA between EC from MGUS and MM. (E) Heatmap representing z-scaled mean regulon activity score of inferred top specific regulons for EC in each stage. (F) Density plots showing the activity score of Xbp1 and Sox18 regulons in EC.

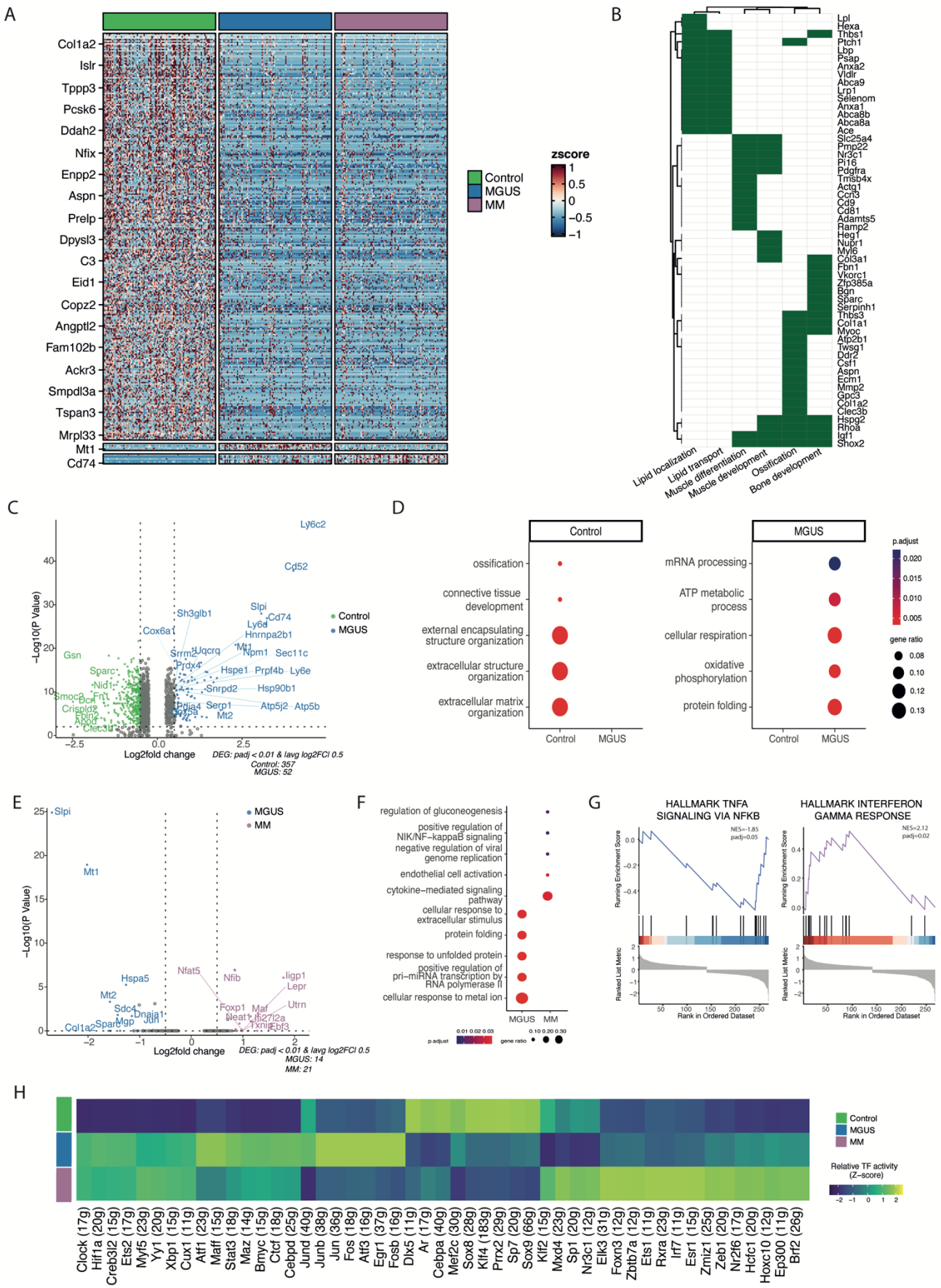

Figure 4. MSC undergo early transcriptional changes during pre-malignant MGUS that persist in overt MM. (A) Heatmap depicting DEG between MSC in control, MGUS, and MM. Color represents the z-score scaled expression values. (B) Heatmap of significantly downregulated GO terms in MGUS and MM cells

compared to control MSC with the associated genes. The green color represents the presence of the gene in each GO term. (C) Volcano plot of the DEGs from the comparison between MSC from control and MGUS. The y-axis represents the -log10(p-value), and the x-axis represents the log2(fold change) of the gene. The dot's color denotes the disease stage for which DEG was detected, with grey dots representing non-significant genes. (D) Significant terms derived from ORA of MSC from control vs MGUS. (E) Volcano plot of the DEGs in MSC from MGUS vs. MM. (F) ORA between MSC from MGUS and MM. (G) GSEA plots for the gene sets 'TNFα signaling via NFκB' (left panel) and 'Interferon gamma response' (right panel) in MGUS vs MM MSC. (H) Heatmap of mean regulon activity score of significantly enriched regulons in each stage. The color scale represents the z-score of the activity scaled by row.

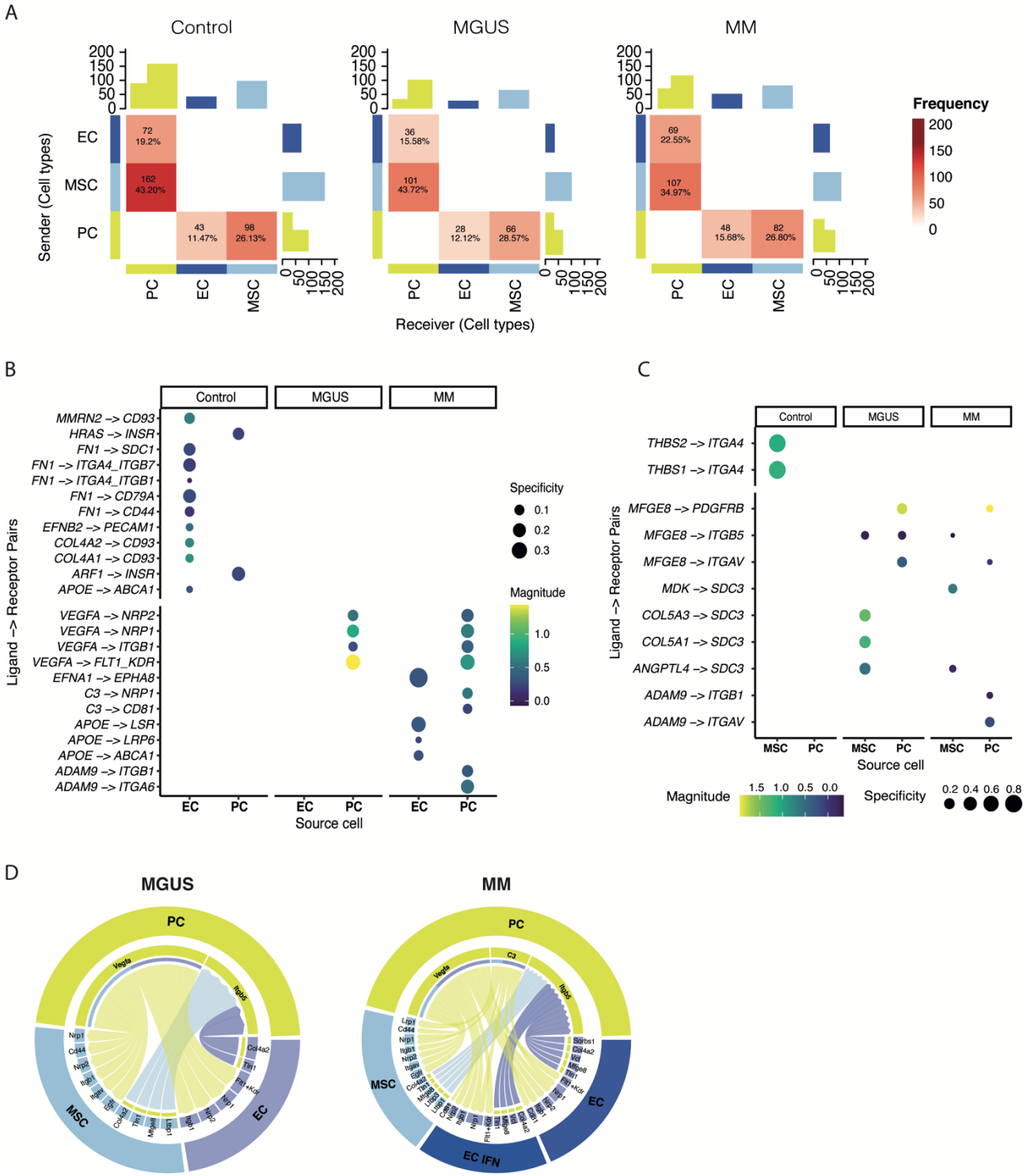

Figure 5. Altered crosstalk between EC and MSC with malignant PC is potentially associated to

myeloma development (A) Heatmap showing the number of predicted cellular interactions between EC, MSC and PC. Block sizes and colors are proportional to the number of ligand-receptor pairs. (B-C) Dot plots of representative ligand-receptor interactions between PC and EC (B) or MSC (C) during disease progression. Dot size and color indicate the specificity and the strength of the interaction, respectively. (D) Chord diagram showing shared relevant signaling network between EC, MSC, and malignant PC in the MGUS and MM stages. Colors and width represent signal senders and strength, respectively.

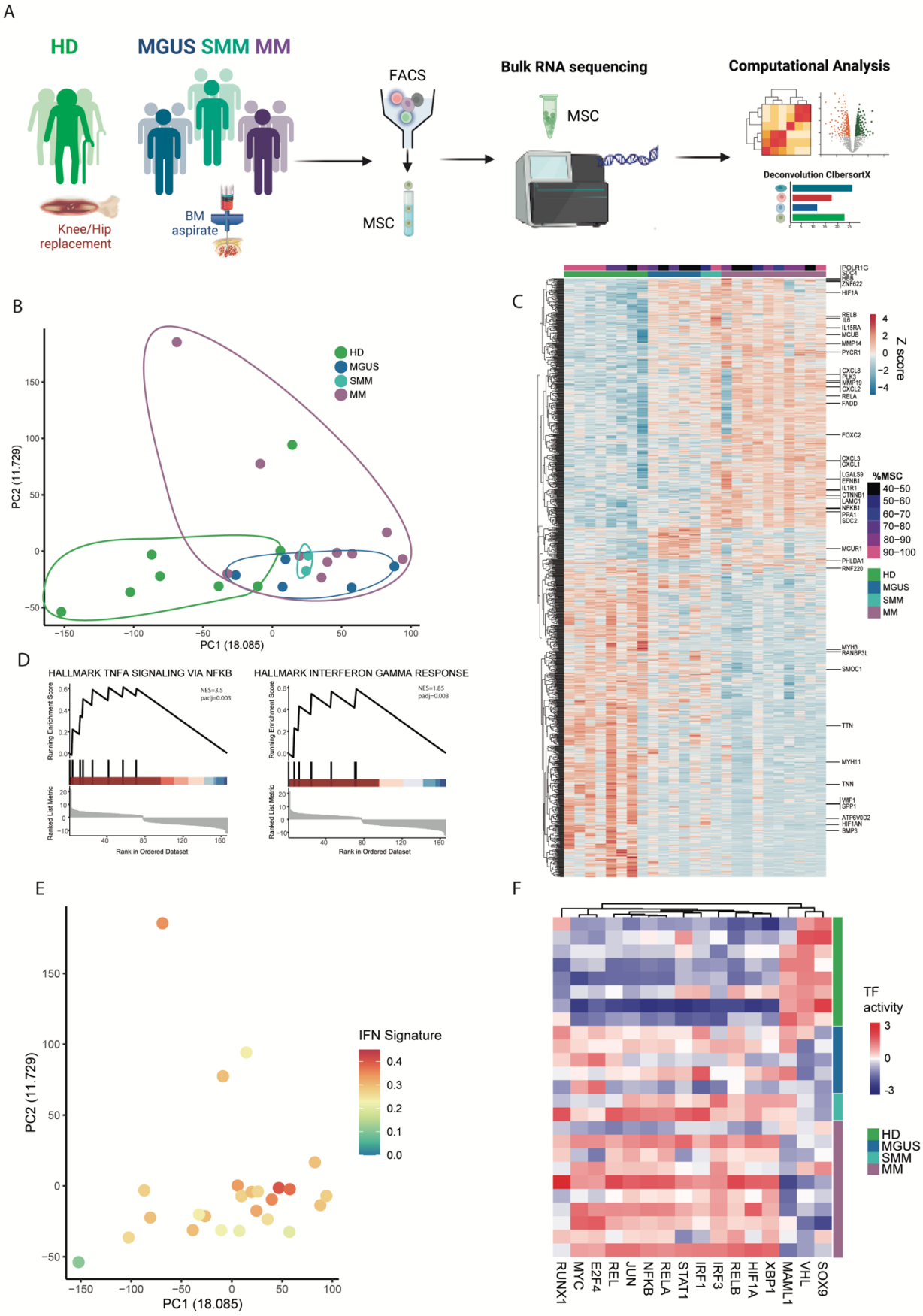

Figure 6. Transcriptional dynamics of human MSC during myeloma progression. (A) Experimental workflow used for the isolation and bulk RNA-seq analysis of human BM MSC. (B) PCA of MSC expression

profiles shows clustering by disease stage. The color of the dots represents disease stages. (C) Heatmap showing the expression profiles across samples of DEGs identified in each pairwise comparison along disease progression. (D) GSEA plots for the gene sets 'TNFα signaling via NFκB' (left panel) and 'Interferon gamma response' (right panel) in the comparison between HD- MSC and MM-MSC. (E) PCA plot showing the MM-IFN signature score in each human sample, previously identified murine BM MM cells. (F) Heatmap representing the variation of TF activity score across samples.